Ordered CdS nanorods - organic hybrid solar cells

Yoonmook Kang*, Donghwan Kim

Abstract We studied the optoelectronic properties of hybrid solar cells formed by mixing cadmium sulfide (CdS) nanorods with a conjugated polymer, poly-2-methoxy,5-(2'-ethylhexyloxy)-1,4-p-phenylenevinylene (MEH-PPV). CdS nanorods were grown vertically on Ti substrates by electrochemical deposition through a porous alumina template. Absorption spectrum of the composite layer was the same as the superposition of the absorption spectrum of each individual layer. The photoluminescence signal from MEH-PPV film was reduced as a result of the mixing. The energy conversion efficiency of MEH-PPV improved from 0.0012% to about 0.60% when combined with the vertically aligned CdS nanorods.

Key words Photovoltaic, hybrid solar cell, organic, nanorod, CdS

* Division of Materials Science and Engineering
■ Korea University, Anam-dong, Seongbuk-gu, Seoul 137 - 713, Korea
■ E-mail : ddang@korea.ac.kr ■ Tel: +82 2 3290 3713 ■ Fax: +82 2 928 3594

Organic conjugated polymers exhibit the optoelectronic properties of semiconductors as well as the mechanical properties and the processing advantages of polymeric materials. They can be deposited from solution at low temperatures onto, e.g.; flexible substrates, using simple and inexpensive deposition methods such as spin or blade coating. However, the power conversion efficiency (PCE) of organic solar cells is limited by the low dissociation probability of excitons and the inefficient hopping carrier transport [1]. The best efficiencies were achieved when the pure polymer active layer was replaced by a blend layer [2]. Among various types of organic solar cells, the organic-inorganic hybrid solar cell is one of the most promising type since it not only has a large interface area where excitons, the bound electron-hole pairs, may effectively dissociate but also has two separate channels for efficient electron and hole transport, i.e., the semiconductor nanorods and the polymer layers, respectively.

In 1993 Sariciftci et al. reported a high fill factor of 0.48 and PCE of 0.04% under monochromatic illumination in the hybrid solar cells of fullerene and conjugated polymer, and explained the improved performance by fast electron injection from the photoexcited state of conjugated polymer into fullerene that should result in the efficient charge separation at the large donor/acceptor interfacial area [3]. In 2002 E. Kymakis et al. also investigated the heterojunctions where the single-wall carbon nanotubes (SWNT) should be the pathway for the electrons [4]. This device has the advantage of reducing the number of hopping between fullerenes for electron transport. Further improvement of hybrid solar cell was reported by Alivisatos et al. combining CdSe nanorods with poly(3-hexylthiophene)(P3HT) [5]. Their devices showed an open circuit voltage of 0.7 V, a short circuit current of 5.7 mA, a fill factor of 0.4 and a power conversion efficiency of 1.7% under the air mass 1.5. Compared to the earlier hybrid devices, their cells have the advantage of the improved optical absorption in the visible range by the semiconductor

nanorods. The photovoltaic performance of the devices may still be improved if the nanorods are aligned vertically between the two electrodes to minimize the carrier transport paths and if various nanorod materials are tested for optimization. However both the fabrication and the alignment of nanorods with different materials are difficult tasks. Electroplating on porous alumina membrane should be a relatively easy process by which to obtain aligned nanorods [6]. In this paper, we studied the fabrication and characterization of CdS nanorod/MEH-PPV hybrid solar cells. Although there was a report on CdSe nanorods/MEH-PPV hybrid solar cells [7], to our best knowledge, this is the first attempt to construct heterojunction solar cells with vertically aligned CdS nanorods as an efficient electron acceptors when blended with the conjugated polymer.

CdS nanorods were deposited electrochemically on anodic alumina membrane (AAM) substrate. The AAM used in this work were prepared via a two-step aluminum anodic oxidation process in a 0.2 M phosphoric acid electrolyte at 25℃ at a constant current density 100 μA/ cm^2 [8]. The diameter, length, and density of the AAM pores were about 200 nm, 30 μm, and 5×10^8/cm^2, respectively. After the anodization, each samples were removed from the electrolyte, washed in distilled water and dried in a nitrogen gas. Then a titanium layer was evaporated onto one side of the AAM for to be used as the working electrode. CdS nanorods were cathodically deposited in an aqueous solution of 0.2M $CdSO_4$ and 0.01M of $Na_2S_2O_3$ adjusted to a pH of 2~3 using concentrated hydrochloric acid. A static potential of -0.8 V was applied with respect to a standard calomel electrode during the deposition process [9-11]. After the electrochemical deposition, and the alumina template was dissolved in 1 M NaOH at 25℃ for 1 h and was rinsed several times in D.I. water [8].

The photoactive layer was formed by spin coating of a MEH-PPV solution from a 1mg/ml chloroform solution onto CdS-nanorod substrate. Thermal annealing of the sample was performed in a vacuum chamber at elevated temperatures (100℃) under formimg gas (a mixture of 90% Ar (99.9999%) and 10% H_2 (99.999%)) atmosphere [12]. This method suppresses the formation of carbonyl defects during the thermal treatment in air that reduces the conjugation length and thus lowers the electrical conductivity when oxidized [13]. Finally the Au front electrodes were vacuum-deposited through a shadow mask. In order to minimize an aging effect due to

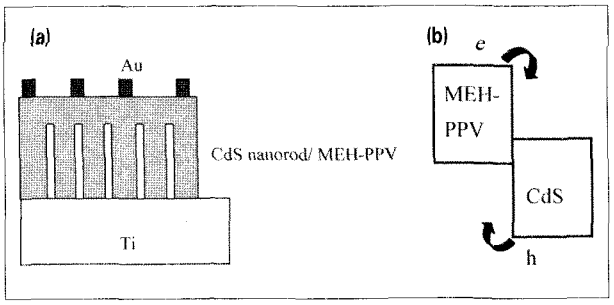

Fig. 1 (a) The structure of CdS nanorods/MEH-PPV hybrid solar cells. (b) The energy band diagram and the expected charge separation direction in the interface region.

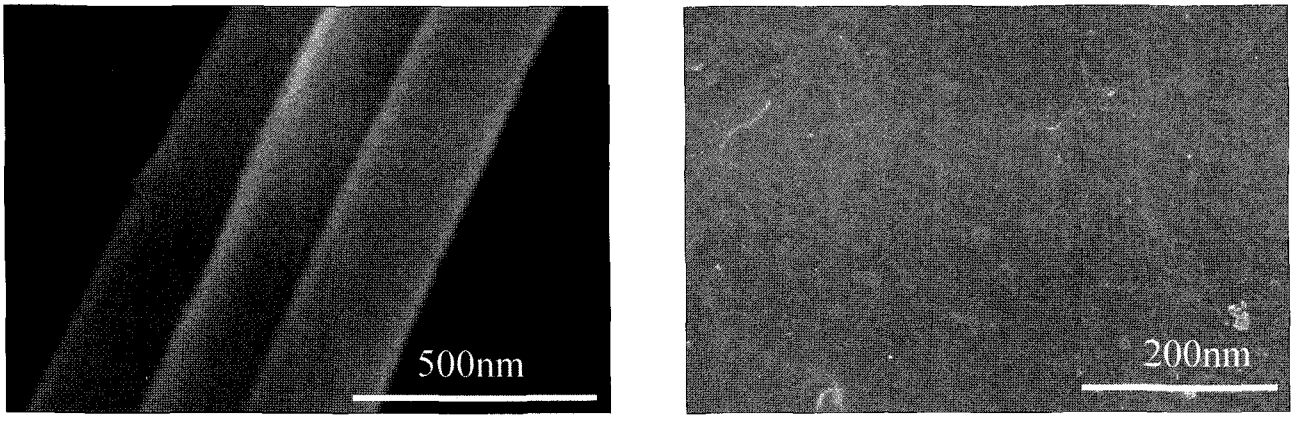

(a) (b)

Fig. 2 SEM image of the CdS nanorods produced by electrochemical deposition (a), and the surface of the MEH-PPV/CdS nanorod composite layer (b).

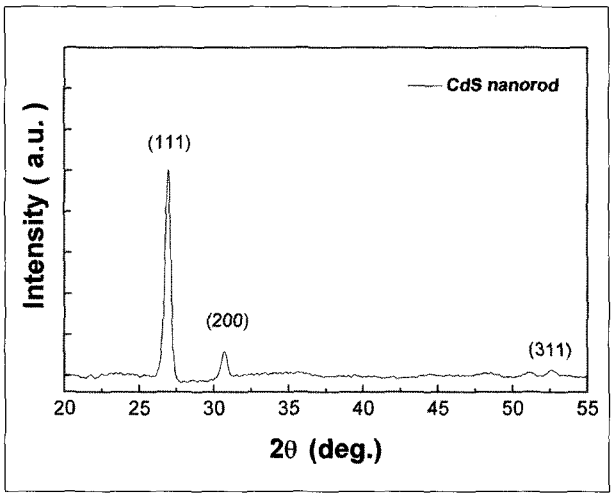

Fig. 3 XRD pattern of CdS nanorods.

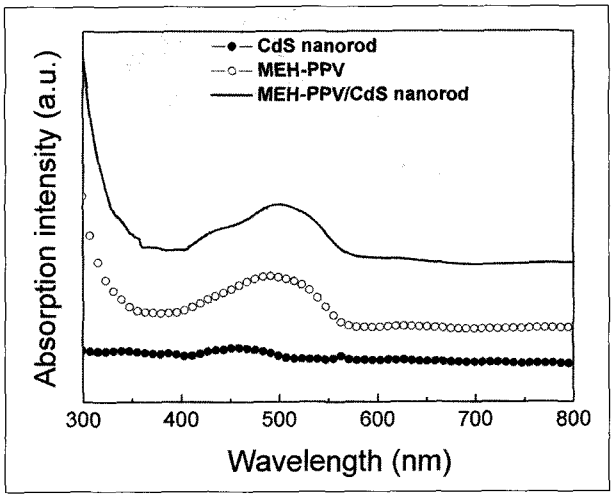

Fig. 4 Absorption spectra of MEH-PPV/CdS nanorods, MEHPPV, and CdS nanorods, respectively

oxygen or moisture, the devices were kept in a nitrogen-filled chamber after the preparation. The films were protected from blue and ultraviolet light except during the measurements. The nanorods and the device surface were observed by field emission scanning electron microscopy (FESEM). The crystal structures of the CdS nanorods were investigated by x-ray diffraction (XRD) using Cu Kα radiation. Absorption spectra were measured by a Hewlett-Packard 8453 UV-Vis spectrophotometer.

The photoluminescence (PL) efficiency was determined using an integrating sphere coupled to an Oriel InstaSpec IV spectrophotometer via a liquid light-guide. The samples were excited by an argon ion laser at a wavelength of 488 nm with a power of approximately 1mW. Electrical data were taken using a Keithley 2400 source-measure unit. The devices were tested under dark and illuminated conditions (nominal air mass 1.5 condition of 100 mW/cm^2) at 25℃ through the Au front electrode side.

A schematic description of our device is displayed in Figure 1. It can be seen that CdS nanorod is electron-accepting and MEH-PPV is hole-accepting (Fig. 1b). CdS is used as the electron transport channel whereas MEH-PPV is an effective hole transport material.

An image of CdS nanorods is shown in Figure 2(a). CdS seemed to uniformly fill the pores in AAM substrate, and thus reproduce the shape of the membrane pores. The diameter, length, and density of the CdS nanorods were about 200 nm, 30 μm, and 5 $\times 10^8$/cm^2, respectively, that are essentially the same as those of the pores in AAM substrates.

A surface image of the CdS nanorods/MEH-PPV layer is shown in Figure 2(b). It can be found that CdS nanorods are well embedded in the MEH-PPV matrix. The thickness of the photoactive layer was about 20 μm.

The crystallographic structure of the CdS nanorods was determined by XRD (Figure 3). The XRD pattern contains three peaks that are clearly distinguishable. All of them can be indexed to crystalline CdS (JCPDS card, no. 10-0454). The 2θ values of diffraction peaks observed are 26.5°, 30.8°, and 52.1°, they correspond to the reflections from (111), (200), and (311) planes of cubic (zinc blende) CdS.

Figure 4 shows the absorption spectra between the wavelength of 300 and 1000 nm for the CdS nanorods and polymer composite samples used in this work. The optical absorption spectrum of a pure MEH-PPV film has an absorption edge at 590 nm and the maximum at 500 nm in the visible portion of the spectrum. The peak of the MEH-PPV film is in good agreement with the reported value [14-15]. For CdS nanorods, the absorption starts a slow rise around 500 nm, followed by a peak at 460 nm. Correcting for the reflection loss, the optical density of MEH-PPV/CdS nanorod composite film is the superposition of the two types of materials. In other words,

the spectrum from the composite layer is simply the sum of the absorption spectra of the constituent parts of the composite films with no additional peaks in 300-800 nm range.

In order to achieve the efficient solar cell, a fast dissociation of excitons is required at the donor-acceptor interface. An effective dissociation is only possible for the excitons that are created within about 10 nm, the typical diffusion length of excitons, from the interface [16]. Thus, we investigated the exciton transport behavior in MEH-PPV/CdS nanorod heterojunction by comparing its PL intensity with that of the MEH-PPV film (see Fig. 5).

The PL peaks of the pure MEH-PPV film are observed around 580 and 640 nm. The PL intensity of the MEH-PPV/CdS nanorod composite film is significantly reduced to 0.02 times the value of the MEH-PPV film. This PL quenching provides an evidence for exciton dissociation, because, once the photogenerated excitons are dissociated, the probability for recombination should be significantly reduced. This is a well known effect of the ultrafast electron transfer from the donor to acceptor and it is expected to increase the exciton dissociation efficiency in photovoltaic devices [17-19].

The dynamics of the PL decay for the same samples are shown in Fig. 5(b). As one can see from Fig. 5(b), even though the annealing condition for all the samples is the same, the PL transients are very different [19-20]. The PL decay profiles of MEH-PPV/CdS nanorod film and MEH-PPV film show different behaviors which can be fitted with single exponential function with estimated lifetime of 52.4 and 92ps, respectively. PL from MEH-PPV sample decays significantly slower compared to that from the MEH-PPV/CdS nanorod sample. We suggest that the PL decay should be affected by exciton dissociation at the MEH-PPV/CdS nanorod interface rather than annealing-induced levels such as carbonyl defect.

Figure 6 shows the results of current density versus voltage measurements on the devices made in this study. When a pure MEH-PPV layer was sandwiched between the two electrodes, no junction characteristics were apparent probably due to the high electrical resistivity of the material. The rectifying behavior was observed when CdS nanorods were added to MEH-PPV. The short-circuit current, open-circuit voltage, fill factor, and power conversion efficiency were

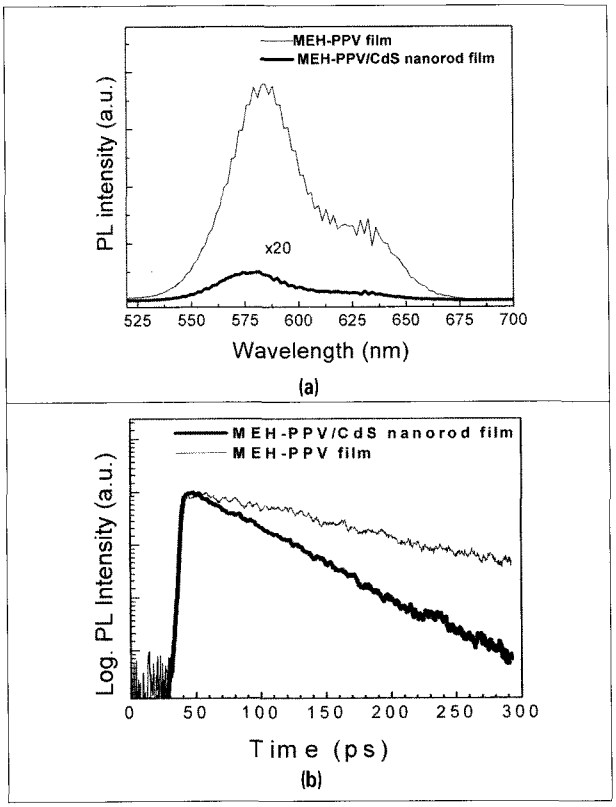

Fig 5 (a) Photoluminescence spectra at room temperature with excitation at 488 nm for annealed MEH-PPV and annealed MEH-PPV/CdS nanorods, respectively.
(b) Normalized PL decays for the same samples.

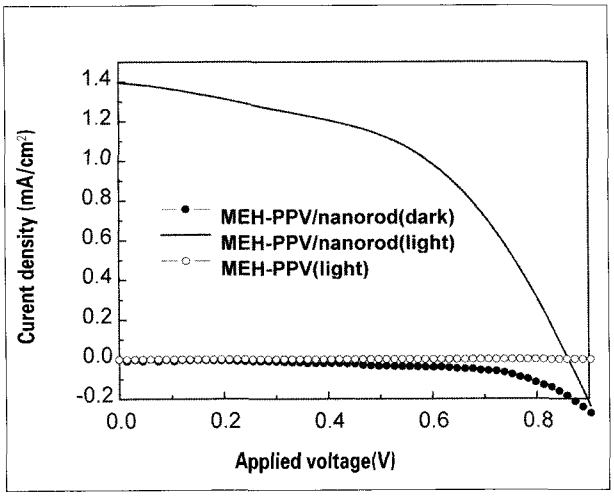

Fig. 6 Plot of the current density versus applied voltage for the devices operated in the dark and under illumination of 100mW/cm².

1.397 mA/cm^2, 0.858 V, 0.496, and 0.60%, respectively. For a pure polymer device, the efficiency was only 0.0012%. Our results indicate that the use of nanorods should be an effective route to achieve high efficiencies by inducing the exciton dissociation and enhancing the electron transport in crystalline paths perpendicular to the plane of the film. Further improvements in efficiency are likely to involve (i) adopting a semiconductor material with an ideal band gap for absorbing solar spectrum such as cadmium telluride, (ii) controlling the electrical characteristics of the semiconductor/polymer interfaces, and (iii) optimizing the constituent materials in terms of the charge transport.

In conclusion, we have demonstrated that a significant improvement in photovoltaic characteristics of polymer solar cells should be achieved when vertically aligned semiconductor nanorods are added. The interface between a conjugated polymer and semiconductor should provide an efficient charge separation for photogenerated excitons. The nanorods function as the efficient path for electron transport. The use of nanorods is expected to provide a great flexibility in controlling the performance of photovoltaic devices.

Reference

1. H. Bassler, Molec. Crys. Liq. Crys. Sci. Technol. Sec. A252, 11 (1994).
2. Franz Padinger, Roman S. Rittberger, and Niyazi S. Sariciftci, Adv. Funct. Mater. 13, 85 (2003).
3. N. S. Sariciftci, D. Braun, and C. Zhang, V. I. Srdanov, A. J. Heeger, G. Stucky, and F. Wudl, Appt. Phys. Lett. 62, 585 (1993)
4. E. Kymakis and G. A. J. Amaratunga, Appl. Phys. Lett. 80, 112 (2002)
5. Wendy U. Huynh, Janke J. Dittmer, A. Paul Alivisatos, Sciencs 295, 2425 (2002)
6. N. Kouklin, L. Menon, A. Z. Wong, D. W. Thompson, J. A. Woollam, P. F. Williams, and S. Bandyopadhyay, Appl. Phys. Lett. 79, 4423 (2001).
7. Wendy U. Huynh, Janke J. Dittmer, Nerayo Teclemariam, Delia J. Milliron, and A. Paul Alivisatos, PRB 67, 115326 (2003)
8. H. Masuda, M. Satoh, Jpn. J. Appl. Phys., Part 2 35, L 126 (1996)
9. L. P. Colletti, D. Teklay, and J. L. Stickney, J. Electroanal. Chem. 369, 145 (1994).
10. M. Innocenti, G. Pezzatini, F. Forni, and M. L. Foresti J. Electrochem. Soc. 148, C357 (2001)
11. Dmitri Routkevitch, Terry Bigioni, Martin Moskovits, and Jing Ming Xu, J. Phys. Chem. 100, 14037 (1996)
12. F. Papadimitrakopoulos, Konstadinidis, T. M. Miller, R. Opila, E. A. Chandross, and M. E. Galvin, Chem. Mater. 6, 1563 (1994)
13. M. Yan, L. J. Rothberg, F. Papadimitrakopoulos, M. E. Galvin, T. M. Miller, Phys. Rev. B 73, 744 (1994)
14. Thuc-Quyen Nguyen, Vinh Doan, and Benjamin J. Schwartz, J. Chem. Phys.110, 4068 (1999)
15. Tung-Wah Frederick Chang, Sergei Musikhin, Ludmila Bakueva, Larissa Levina, Margaret 16. Thomas Stubinger and Wolfgang Brutting, J. Appl. Phys. 90, 3632 (2001)
17. Ji Yu, Dehong Hu, Paul F. Barbara, Science 289 , 1327 (2000)
18. Gregory D. Scholes, Delmar S. Larsen, Graham R. Fleming, Garry Rumbles, and Paul L. Burn, Phys. Rev. B 61, 13670 (2000)
19. G. Yu and A. J. Heeger, J. Appl. Phys. 78, 4510 (1995)
20. N. S. Sariciftci, D. Braun, C. Zhang, V. Srdanov, A. J. Heeger, G. Stucky, and E Wudl, Appl. Phys. Lett. 62, 585 (1993).

강 윤 묵

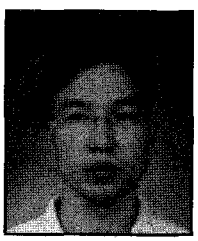

2000년 동국대학교 반도체과학과 이학사
2002년 동국대학교 반도체과학과 이학석사
2004년 고려대학교 신소재공학과 공학박사수료

현재 박사과정(고려대학교)
반도체응용연구실(신소재공학과)
(E-mail : ddang@korea.ac.kr)

김 동 환

1982년 서울대 공과대학 금속공학과
1984년 서울대 공과대학 금속공학과 대학원
1993년 스탠포드 대학교 재료공학과 공학박사 수료

현재 고려대학교 재료공학부 교수
(E-mail : donghwan@korea.ac.kr)